frontiers | Frontiers in Astronomy and Space Sciences

TYPE Original Research
PUBLISHED 19 September 2022
DOI 10.3389/fspas.2022.823227

Check for updates

OPEN ACCESS

EDITED BY
Jun Yang,
Peking University, China

REVIEWED BY
Xinting Yu,
University of California, Santa Cruz, United States
Nigel John Mason,
University of Kent, United Kingdom

*CORRESPONDENCE
Danica Adams,
djadams@caltech.edu

SPECIALTY SECTION
This article was submitted to Exoplanets, a section of the journal Frontiers in Astronomy and Space Sciences

RECEIVED 26 November 2021
ACCEPTED 31 August 2022
PUBLISHED 19 September 2022

CITATION
Adams D, Luo Y and Yung YL (2022), Hydrocarbon chemistry in the atmosphere of a Warmer Exo-Titan. *Front. Astron. Space Sci.* 9:823227. doi: 10.3389/fspas.2022.823227



# Hydrocarbon chemistry in the atmosphere of a Warmer Exo-Titan

Danica Adams[1]*, Yangcheng Luo[1] and Yuk L. Yung[1,2]

[1]Division of Geological and Planetary Sciences, California Institute of Technology, Pasadena, CA, United States, [2]Jet Propulsion Laboratory, La Cañada Flintridge, CA, United States

Hosting a ~1.5 bar $N_2$ atmosphere and reducing atmospheric composition, Titan has the energy sources needed to drive disequilibrium chemistry and hosts an aerosol layer which shields the surface from incident UV radiation. This world draws parallels to an early Earth-like world (although ~200 K cooler), and the atmospheric chemistry may be capable of forming relevant prebiotic species. Exo-Titan worlds at close-in orbits host photochemistry relevant to habitability with rich hydrocarbon chemistry. We investigate the effect of stellar type of the host star, equilibrium temperature, incident radiation, and vertical transport efficiency on the production of higher-order hydrocarbons. We find a greater incident radiation (a closer orbit) increases the rate of methane photolysis as well as photolysis of hydrocarbons. A larger $H_2$ abundance and warmer temperature increases the rate of the back reaction $H_2 + CH_3 \rightarrow CH_4 +$ H, and the temperature dependence is so great that $CH_3$ recycles back into $CH_4$ instead of forming $C_2H_6$. A larger $H_2$ abundance and warmer temperature also encourages interesting cycling between $C_2H_2$, $C_2H_3$, and $C_2H_4$ *via* reactions with atomic H.

KEYWORDS
**hydrocarbon, exoplanet atmosphere, titan, photochemistry, exoplanet astronomy**

## 1 Introduction

Titan is the only solar system body demonstrated to have complex organic chemistry occurring in an Earth-like atmospheric envelope (~1.5 bar), which is a result of its unique atmospheric properties: A $N_2$ atmosphere with a reducing composition, energy sources to drive disequilibrium chemistry, and an aerosol layer to shield the surface from solar UV radiation (e.g., Yung et al., 1984; Wilson and Atreya, 2004; Willacy et al., 2016). This world draws parallels to an early Earth-like world which may have been reducing (e.g., Lunine 2005; Lorenz and Mitton 2008), and these characteristics make it an appealing object of study when exploring planetary habitability.

To date, over 5,000 exoplanets have been discovered, primarily due to NASA's *Kepler* mission which searched for and discovered transiting exoplanets. Hot-Jupiters were the easiest planets to detect at first, but today small (1–4 Re), low mass (<20 Me) and short period (of less than 100 days) planets are the most common type of exoplanet known today (e.g., Bean et al., 2020). The atmospheres of small close-in planets are vulnerable to rapid escape; however, it has been recently suggested that during planet formation of super-Earth planets, $H_2$ may not have accumulated as a thick gaseous envelope, but instead would dissolve in the interior magma (Chachan and Stevenson, 2018; Kite et al., 2020). Outgassing of a reduced secondary atmosphere may be plausible and has been suggested to explain the observed atmospheric spectra of GJ 1132b, a super-Earth orbiting an M-Dwarf at a close-in orbit at 0.01 AU, a super-Earth orbiting an M-Dwarf at a close-in orbit at 0.01 AU (Swain et al., 2021). Recent Hubble Space Telescope (HST) observations suggest a surface pressure between 1 and 10 bars, a surface temperature of 950 K, a stratospheric temperature of ~480 K, and an $H_2$-dominated atmosphere with nitrogen and hydrocarbon chemistry (Swain et al., 2021). Although, recent works have also disputed the observations, suggesting either that photochemical hazes muted the spectral features or that no atmosphere was present (Libby-Roberts et al., 2021; Mikal-Evans et al., 2021).

The photochemistry in the reduced atmospheres of close-in, rocky planets may be unique from the solar system worlds. Previous studies have primarily examined the surface climate and atmospheric circulation of Earth-like exoplanets (e.g., Merlis and Shneider 2010; Kopparapu et al., 2013; Shields et al., 2013; Kaspi and Showman 2015; Shields et al., 2016), but fewer investigations have explored the range of possible conditions at exoplanets with photochemical hazes, reduced atmospheres, and/or different equilibrium temperatures. Morley et al. (2015) considers the photochemical production of aerosol precursors, as well as cloud distribution and synthetic spectra, over a wide range of stellar irradiances, metallicities, and aerosol sedimentation rates. Lora et al. (2018) examines the response of a Titan-like atmosphere to different host stars and finds (in agreement with results presented here in Section 3) that the greater shortwave activity but lower luminosity of M-Dwarves both result in a lesser production of hydrocarbons. Motivated by GJ 1132b, here we investigate the response of a Titan-like atmosphere to a larger swath of planetary parameters than previously considered in order to more closely adapt known atmospheric chemistry to the conditions of close-in super-Earths: to a warmer temperature, larger irradiation flux, different stellar type, and different background $H_2$:$N_2$ ratios. We term these planets exo-Titan due to their similarities in atmospheric composition (reduced, N-bearing chemistry), although we acknowledge the differences in interior composition, planetary radius, and temperature.

## 2 Materials and methods

We adapt the Titan KINETICS model presented in Willacy et al. (2022) to various Exo-Titan atmospheres orbiting Sun-like and M-Dwarf host stars. The model considers 111 species linked by 1,143 reactions in order to calculate the chemical production and loss rates at each altitude as well as the diffusive flux between each altitude grid by solving the 1D continuity equation.

We consider Titan and GJ 1132b as our two end members, and consider a swath of theoretical intermediates between in order to examine the photochemical response to four parameters: 1) The stellar type, M-Dwarf vs. K-star vs. Sun-like host star; 2) close-in orbit, ranged from a Titan-like distance of 9.55–0.01 AU; 3) temperature, from a Titan temperature (94 K at the surface and 170 K in the stratosphere) to a GJ 1132b temperature (950 K at the surface and 480 K in the stratosphere); and 4) initial $H_2$:$N_2$ ratio, varied from Titan-like (or <1% $H_2$) to GJ 1132b-like (10% $N_2$ and 90% $H_2$).

The temperature-pressure (T-P) profile at Titan comes from Willacy et al. (2022), and for orbits at the same equilibrium temperature at different host stars we maintain the same T-P profile. Note however that the stellar spectrum is known to influence the T-P profile through Rayleigh scattering, near-infrared absorption, and convection, and for details about these effects we refer the reader to Eager et al. (2020). The T-P profile at the 9.5 AU at dimmer stars is scaled according to the differing equilibrium temperatures. The T-P profile of GJ 1132b comes from Swain et al. (2021).

The stellar type (M-Dwarf) and properties of GJ 1132 are very similar to those of GJ 1214 (with a temperature of 3000 K and mass of 0.15 solar masses), which is a stellar spectrum that has been well studied. Figure 1 compares the incident radiation at 1 AU of this star and the Sun.

We compute synthetic spectra of the predicted photochemical results in order to consider potential detectability. We use Exo-Transmit (Kempton et al., 2017), an open-source radiative transfer code, that calculates atmospheric transmission spectrum of transiting exoplanets. In this study, we include eleven species—C, $CH_4$, $C_2H_2$, $C_2H_4$, $C_2H_6$, H, HCN, $H_2$, N, $N_2$, and $NH_3$. Then, Exo-Transmit finds atmospheric opacity by interpolating between single-molecule cross section data for $CH_4$, $C_2H_2$, $C_2H_4$, $C_2H_6$, HCN, $N_2$, and $NH_3$ between a predefined temperature-pressure grid (temperature ranging from 100 K to 3000 K with a spacing of 100 K, pressure ranging from $10^{-4}$ Pa–$10^{8}$ Pa with a spacing of one order of magnitude) and collision-induced-absorption opacity data for $CH_4$–$CH_4$, $H_2$–$H_2$, $H_2$–H, $H_2$–$CH_4$, $N_2$–$CH_4$, $N_2$–$H_2$, and $N_2$–$N_2$ between the same temperature grid, solves the radiative transfer equation line by line, and generates wavelength-dependent transit depths. The wavelength range is 300–30 μm. Exo-Transmit considers the oblique path of light through the planetary atmosphere along a distant observer's light of sight. It also accounts for opacity caused by Rayleigh scattering. All opacity data in Exo-Transmit is taken from Freedman et al. (2008), Freedman et al. (2014), and Lupu et al. (2014).

We carry out Exo-Transmit calculations for $10^{-5}$–$10^{3}$ mbar of the modelled atmosphere. Exo-Transmit has a resolving power $\lambda/\Delta\lambda$ of 1,000. For visual clarity, we perform a running average with a resolving power of 50. It is worth noting that some of the modelled atmospheres have altitude ranges with temperatures lower than

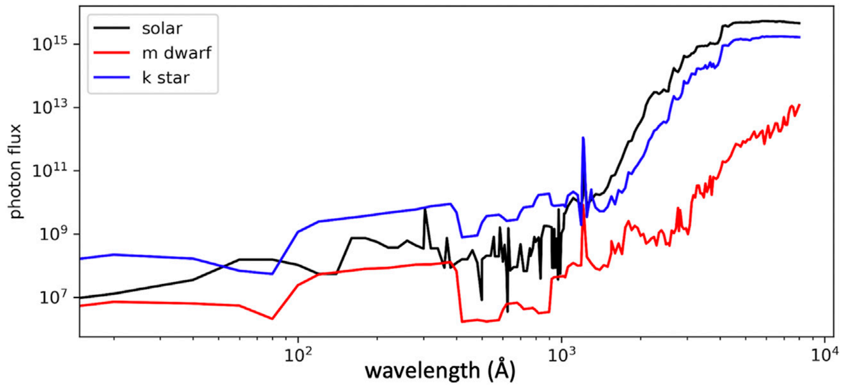


FIGURE 1
Stellar spectra of the Sun (black), an M4.5 host star (red), and a K star (blue), all shown at 1 AU. Photon flux is shown in photons/cm$^2$/s. We obtain the K and M star spectra from the MUSCLES database (France et al., 2016), and we adapt the solar flux from Gladstone et al. (2010). In all cases shown, we have binned to a coarser resolution than the original datasets to minimize model runtime.

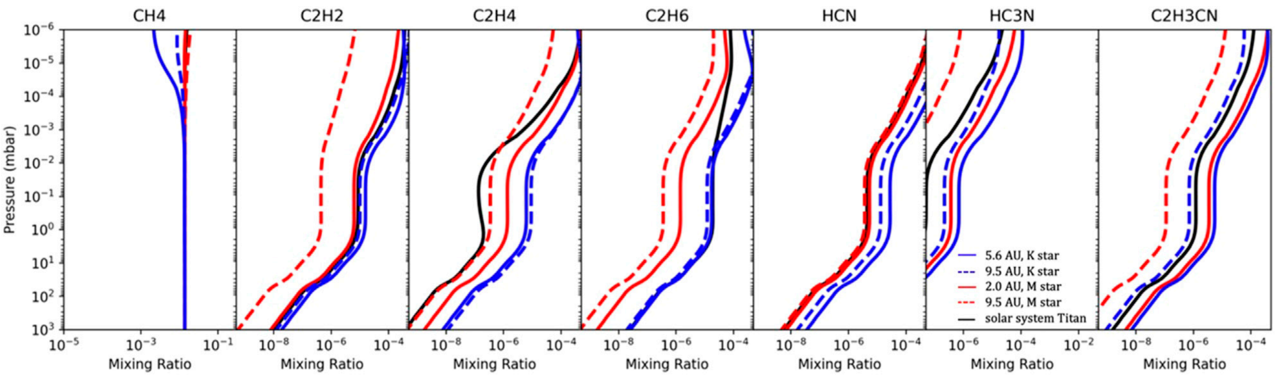


FIGURE 2
Response to stellar type and irradiation; all cases are at a Titan-like temperature and $N_2$-dominated atmosphere. Black line: Sun-like star at 9.55 AU; solid red line: M-Dwarf star at 2.0 AU; dashed red line: M-Dwarf star at 9.5 AU; solid blue line: K star at 5.6 AU; dashed blue line: K star at 9.5 AU. Note that the total irradiation at 2.0 AU from an M-Dwarf host star and 5.6 AU from a K star are both comparable to the total irradiation a world experiences at 9.55 AU from a Sun-like star. From left to right, the panels show $CH_4$, $C_2H_2$, $C_2H_4$, $C_2H_6$, HCN, $HC_3N$, and $C_2H_3CN$.

100 K where Exo-Transmit does not have opacity data. We manually set the opacity for 70–100 K the same as that for 100 K. Sensitivity tests show that the transmission spectra are robust against different approaches of extrapolation.

# 3 Results

## 3.1 Stellar irradiance on hydrocarbon chemistry

The production of hydrocarbons is driven by methane photolysis, which makes the incident photon flux a critical driver of hydrocarbon chemistry. An M-Dwarf host star is more active in the shortwave region than longwave, compared to the Sun. However, the star is less luminous making the total incident radiation at 2 AU orbit comparable to the 9.5 AU orbit around the Sun.

Here, we consider the hydrocarbon chemistry at five worlds: Titan around the Sun, Titan around an M-Dwarf at an orbit of 2 AU and 9.5 AU, and Titan around a K star at an orbit of 5.6 AU and 9.5 AU. The resulting mixing ratios of relevant hydrocarbon species for these cases is shown in Figure 2, and the following sections explain the chemistry driving these results. A similar investigation is presented in Lora et al. (2018), and our results presented in this section largely agree

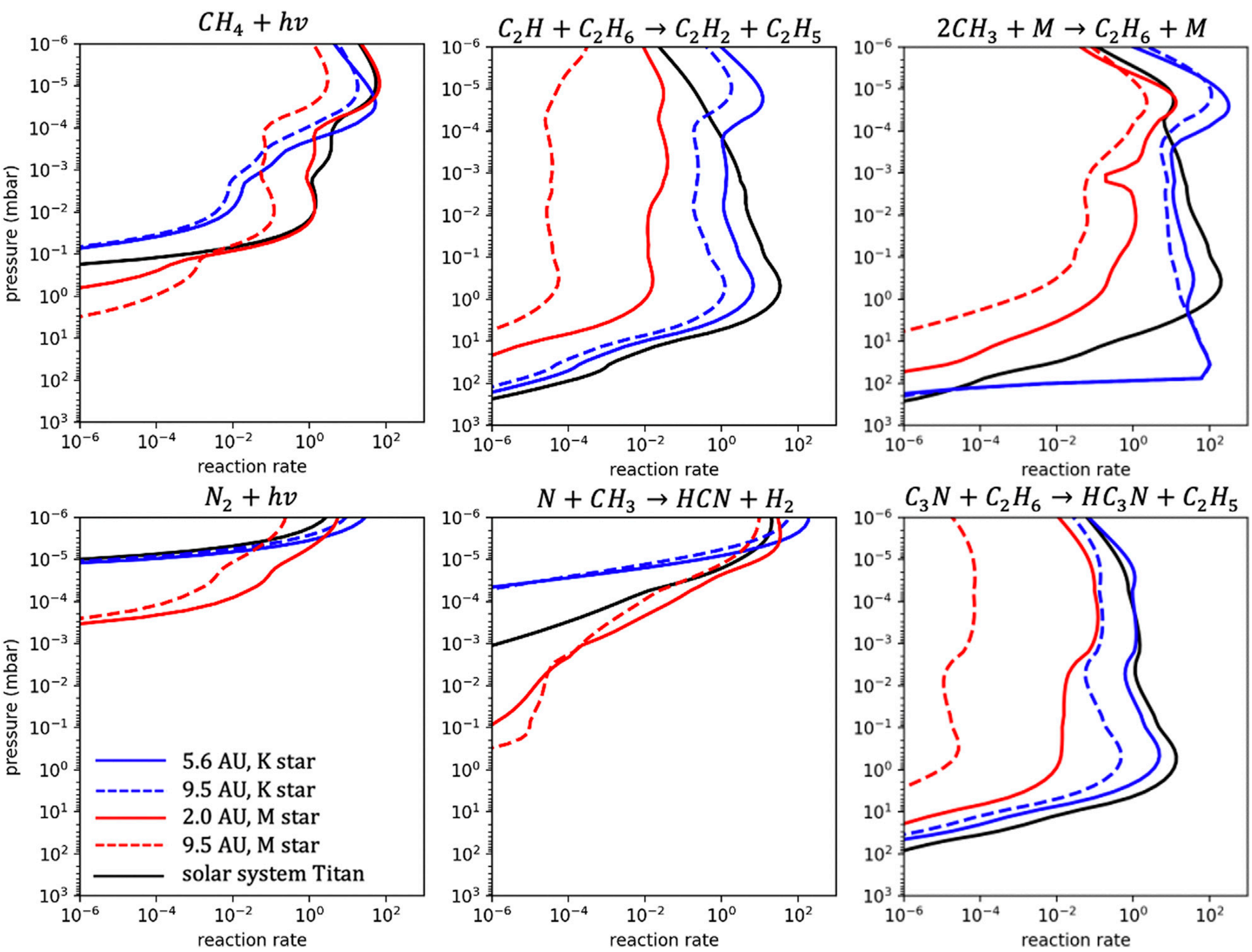


FIGURE 3
Reaction rates ($cm^{-3}\cdot s^{-1}$) of dominant production and destruction reactions for $C_2H_6$. Black lines represent solar system Titan, solid red lines represent Titan around an M-Dwarf at 2 AU, dashed red lines represent Titan around and M-Dwarf at 9.5 AU, solid blue lines represent Titan around a K star at 5.6 AU, and dashed blue lines represent Titan around a K star at 9.5 AU.

with theirs. Understanding these cases is imperative to understanding the novel results presented later in this work.

### 3.1.1 Ethane, $C_2H_6$

At all cases, the production of $C_2H_6$ is dominated by $2CH_3$+M, where M is the third body (Figure 3). At the same equilibrium temperatures (close-in orbits of 5.6 AU and 2.0 AU around the K and M star respectively), the photolysis of methane is comparable to that of Titan around the Sun (Figure 3). However, the enhanced flux of short wavelength ($\lambda < 80\,nm$) photons of the M-Dwarf encourages faster $N_2$ dissociation (Figure 3), allowing N+$CH_3$ (Figure 3) to act as an additional sink of $CH_3$.

At all cases, the dominant loss of ethane are reactions to $C_2H$ and $C_3N$. At a distant orbit of 9.5 AU around an M-Dwarf, methane photolysis is slowed but $N_2$ photolysis is still enhanced, and thus production of ethane is limited. Methane photolysis results from slightly longer wavelength photons (770–1600 A) than $N_2$ photons (680–980 A). A distant orbit means all photon fluxes are reduced compared to a close-in orbit. However, since M Dwarves emit more photons in the smaller wavelengths (relative to longer wavelengths), the slowed photolysis effect is lesser for $N_2$ photolysis. At a distant orbit around a K star, however, dimmer emission at short wavelengths limits $N_2$ photolysis at depth and thereby severely limits N. This slower loss of $CH_3$ allows the $C_2H_6$ production and steady state concentration at a K-star-hosted planet to be more comparable to that at solar system Titan.

### 3.1.2 Acetylene, $C_2H_2$, and ethylene, $C_2H_4$

At Titan, the concentration of acetylene is influenced by production *via* $C_2H$+$CH_4$, and $CH_2$+$CH_2$ balanced by destruction *via* photolysis which yields $C_2H$+H. However, in the upper atmosphere, H+$C_2H_3$ and $CH_3$+$C_2H_3$ and

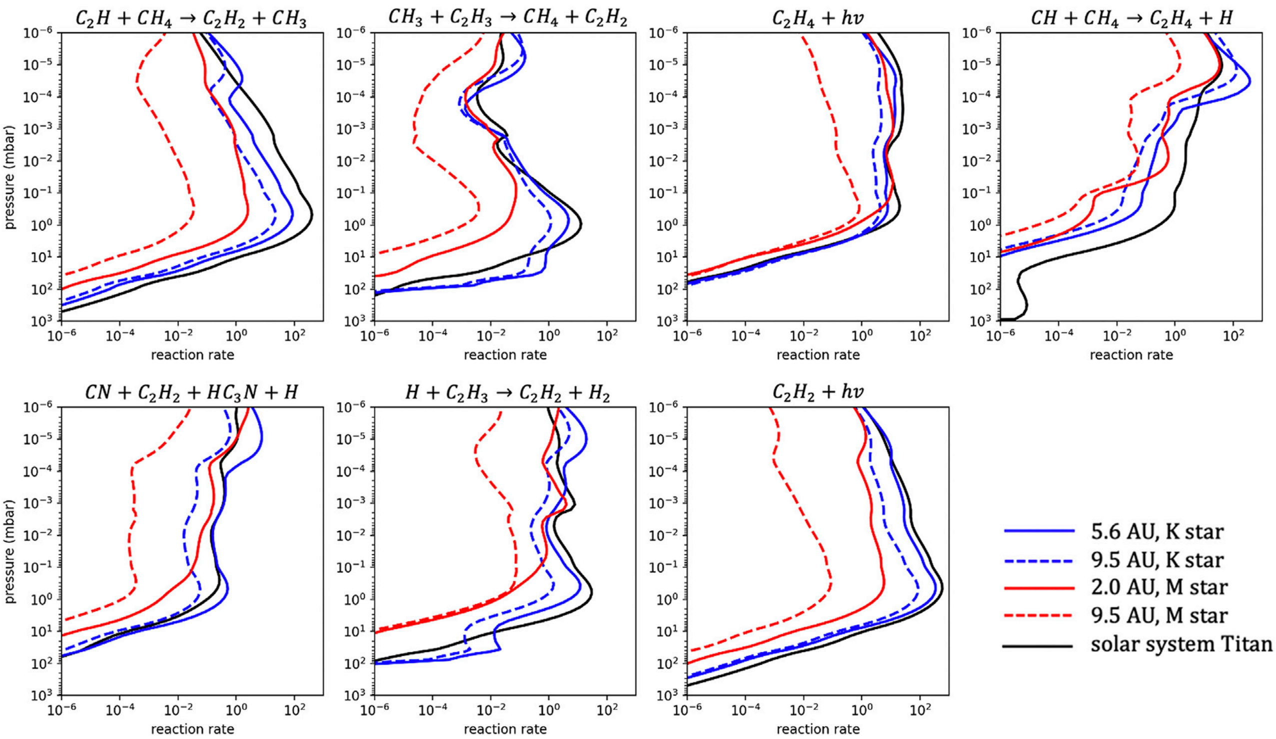


FIGURE 4
Reaction rates ($cm^{-3} \cdot s^{-1}$) of dominant production and destruction reactions for $C_2H_2$ and $C_2H_4$. Black lines represent solar system Titan, solid red lines represent Titan around an M-Dwarf at 2 AU, dashed red lines represent Titan around an M-Dwarf at 9.5 AU, solid blue lines represent Titan around a K star at 5.6 AU, and dashed red lines represent Titan around a K star at 9.5 AU.

$CH_3$+$C_3H_2$ become increasingly relevant as the host star becomes dimmer, where the cycling among $C_2H_2$, $C_2H_3$, and $C_3H_2$ balances the $C_2H_2$ concentration. Additionally, at planets around an M-Dwarf, upper atmospheric $C_2H_2$ is lost to reactions with CN (due to the faster photolysis of $N_2$), while photolysis of $C_2H_2$ remains as the dominant lower atmosphere destruction reaction.

At all cases CH+$CH_4$ is the dominant production, and photolysis is the dominant destruction. At a comparable effective temperature (2 AU around the M-Dwarf), the greater flux of energetic photons results in faster methane photolysis and thereby a faster production of ethylene. From the same distance (9.5 AU), photolysis of both methane (production) and $C_2H_4$ (loss) are slowed and therefore the steady state mixing ratios at Titan and the 9.5 orbit around an M-Dwarf are comparable. Similar trends occur for planets around a K-star; however, the slowing of photolysis rates between the constant effective temperature case and 9.5 AU case is less severe due to the more similar orbit distances presented (only a 4.1 AU change around a K star, but 7.5 AU change around an M Dwarf). The rates of these reactions are compared in Figure 4.

### 3.1.3 -CN species

The greater photon flux in the shortwave spectral region emitted by the M and K stars yields a greater abundance of N and thereby a faster column production of HCN. At the same effective temperature, the planet around the K star hosts the fastest column production of HCN (noticing the fast rate in the upper most region which dominates the column rate). HCN photolysis is driven by lyman-alpha photons, and at the same effective temperatures, the difference in photon flux at these wavelengths causes HCN destruction to be largest at the K star, intermediate at the sun, and smaller at the M star. Generally, HCN is fairly stable to photolysis, so the larger steady state concentration occurs in the case where production is fastest: at the 5.6 AU K star orbit. This planet hosts an ideal combination of fast $N_2$ destruction and abundant hydrocarbons (for N radicals to destroy). Dissociation of $N_2$ and HCN are both faster around the M star than around the sun (see Figure 5), and these effects balance each other out, yielding a comparable HCN concentration as that at solar system Titan.

Photolysis of HCN, the primary loss mechanism, results in CN which may form $C_2H_3CN$ *via* reactions with $C_2H_4$; although, CN may also cycle back to HCN *via* reactions with the hydrocarbons.

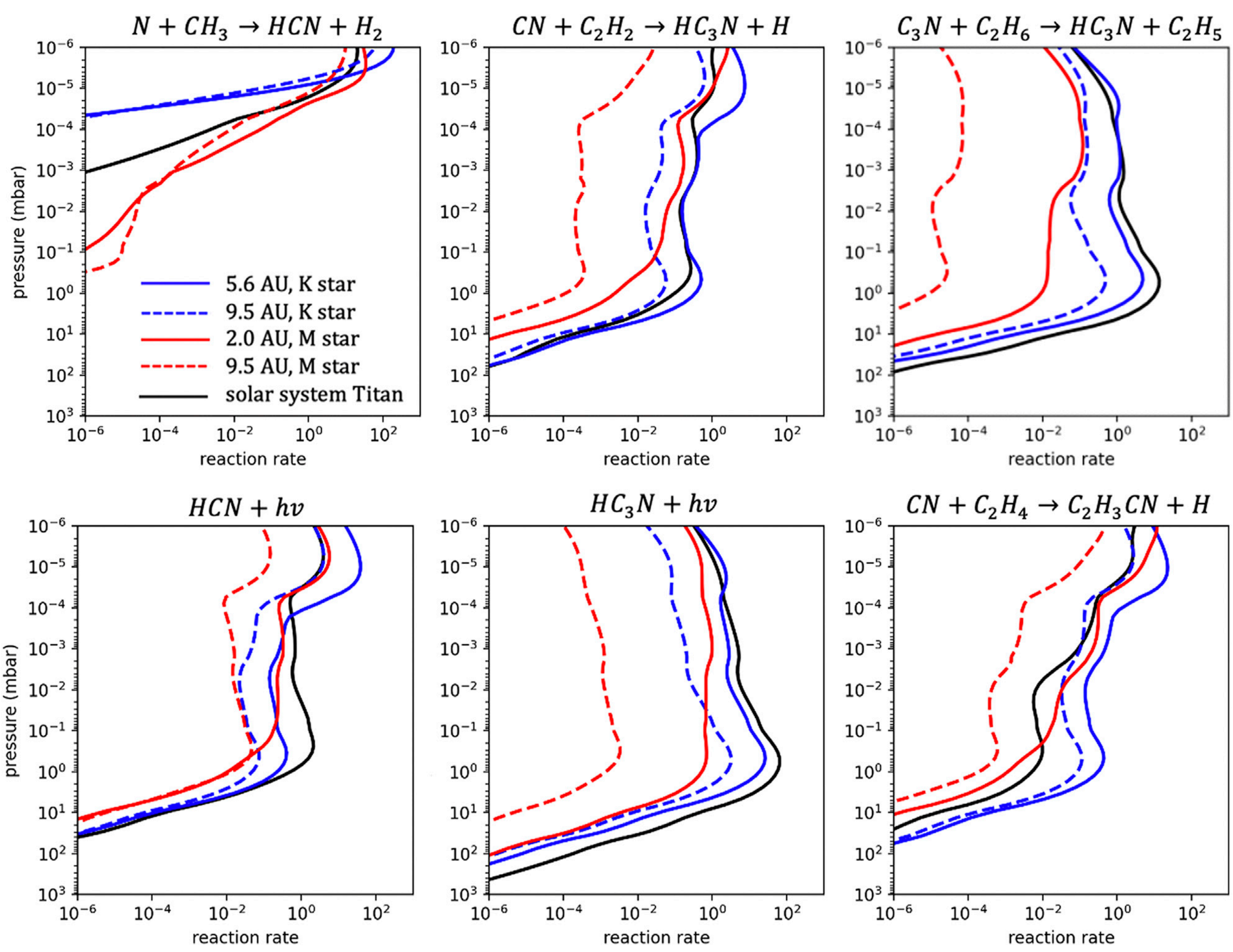


FIGURE 5
Reaction rates ($cm^{-3} \cdot s^{-1}$) of dominant production and destruction reactions for -CN species. Black lines represent solar system Titan, solid red lines represent Titan around an M-Dwarf at 2 AU, dashed red lines represent Titan around an M-Dwarf at 9.5 AU, solid blue lines represent Titan around a K star at 5.6 AU, and dashed red lines represent Titan around a K star at 9.5 AU.

For the same reasons that HCN is larger around the K star at the same equilibrium temperature as solar system Titan (5.6 AU), $HC_3N$ and $C_2H_3CN$ are largest around the K star. Meanwhile, in the 9 AU orbit around the M star, slowed photolysis due to a lower photon flux in total, limits the presence of N and $CH_3$. HCN loss to photolysis is similarly slowed, however, resulting in a similar steady state concentration.

## 3.2 Temperature and $H_2$ composition on hydrocarbon chemistry

With the same solar host star and at the same orbit of 9.5 AU, we now investigate the hydrocarbon chemistry in a cold $N_2$ atmosphere (Titan), a cold $H_2$ dominated atmosphere, and a warm $H_2$ dominated atmosphere (e.g., a sub-Neptune or close-in super Earth). The $H_2$-dominated atmospheres are motivated by the recognized $H_2$-dominated atmosphere of GJ 1132b (Swain et al., 2021) and predicted reduced interiors of close-in super Earths described in Section 1. The temperature-pressure-altitude profiles are shown in Figure 6. The resulting steady state mixing ratios for these cases are shown in Figure 7, and the following sections investigate the chemistry involved.

### 3.2.1 Methane, $CH_4$, and ethane, $C_2H_6$

The reaction $H+CH_4 \rightarrow CH_3+H_2$ is well known to be a mechanism for methane destruction at Titan, other than methane photolysis. Both this reaction and its back reaction, $H_2+CH_3 \rightarrow CH_4+H$, are highly temperature dependent, and in the warmer atmosphere these reactions recycle $CH_3$ back into $CH_4$, which will limit hydrocarbon production. $H+CH_3+M$ is a second important reaction to destroy $CH_3$, and this reaction also

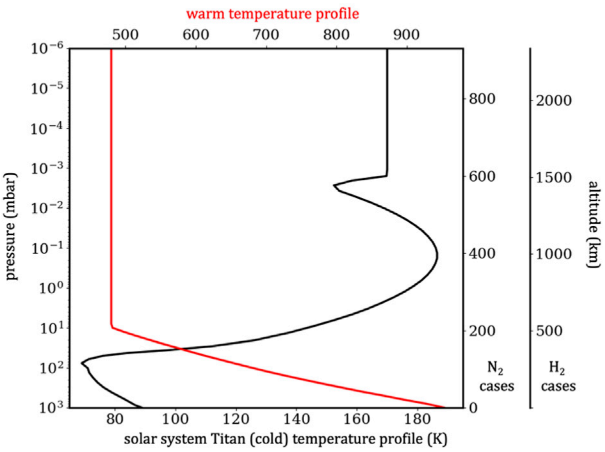


FIGURE 6
Temperature-pressure-altitude profiles of the cold solar system Titan $N_2$ atmosphere (black) and warm Exo-Titan $H_2$ atmosphere (red). Notice the altitude scale changes for the Exo-Titan, which is a result of the warmer temperature and puffy nature (large scale height) of $H_2$ atmospheres.

becomes faster in the $H_2$ atmospheres due to the greater concentrations of H (see Figure 8).

In the $N_2$-dominated atmosphere, photolysis of methane becomes severely photon limited above 0.1 mbar since shortwave photons are lost to $N_2$. In both $H_2$-dominated atmospheres, however, the atmosphere is less opaque to incident stellar photons and photolysis of methane extends down to the near-surface. The $CH_3$ produced from methane photolysis recycles back into methane. However, the photolysis branch of $CH_2$+H acts as a longer-lived sink of methane, and this $CH_2$ may then be photolyzed to CH to kick off subsequent hydrocarbon chemistry described in the following sections.

This cycling does not directly affect the methane profile, but the faster destruction of $CH_3$ is important to the larger hydrocarbons that are shown next.

For all three cases, the production of $C_2H_6$ is dominated by the reaction $2CH_3 \rightarrow C_2H_6$. At Titan, ethane is largely destroyed to reactions with $C_2H$ and secondly to reactions with $C_3N$. However, in an $H_2$-dominated atmosphere, loss is dominated by $H+C_2H_6 \rightarrow C_2H_5+H_2$. The slower production in the warm case in combination with a faster loss rate to atomic hydrogen in both cases (see Figure 8) results in a depleted $C_2H_6$ profile in the $H_2$-dominated atmospheres (as in Figure 7).

### 3.2.2 Acetylene, $C_2H_2$

At Titan, $C_2H_2$ is known to form from $C_2H+CH_4$ in the upper atmosphere and is destroyed *via* photolysis to form $C_2H$+H, and these reactions lead to the autocatalytic destruction of methane. Importantly, $C_2H$ is a chemical product of destruction of larger hydrocarbons, so we note another relevant production of $C_2H_2$ directly from methane photochemical products is $CH+CH_2 \rightarrow C_2H_2+H$. In an H2-dominated atmosphere, the main production of $C_2H_2$ occurs *via* $C_2H+H_2$ instead of with $CH_4$ (as at Titan), and the main destruction is again *via* photolysis to form $C_2H$+H occurs in the upper atmosphere.

In the $H_2$-dominated atmospheres, faster production and loss reactions occur in an inner cycle between $C_2H_2$, $C_2H_3$, and $C_2H_4$ *via* reactions with H and $H_2$. Importantly, this exchange is imperfect; in the full profile $C_2H_2$ reacts to form $C_2H_3$, which cycles back into $C_2H_2$ only in the upper atmosphere. In the middle and lower atmospheres $C_2H_3$ reacts with $H_2$ to build $C_2H_4$ instead of $C_2H_2$. $C_2H_4$ photolysis sources $C_2H_2$ in the middle atmosphere.

In the middle atmosphere, most of these inner cycle reaction rates are comparable to the rates at Titan. However, the photolysis of $C_2H_2$ is faster at Titan due to a larger steady state concentration of $C_2H_2$, and the production of $C_2H_2$ *via* $C_2H+CH_4$ is faster than $C_2H_4$ photolysis (see Figure 9). Therefore, the inner cycle reactions are small compared to the main production/destruction reactions at Titan. At the $H_2$ dominated atmospheres though, the inner cycle is more important, where the photolysis rate is comparable to the inner cycle reaction rates.

### 3.2.3 -CN species

In the mid-atmosphere, HCN loss to $C_2H_3$ becomes faster in the $H_2$-dominated warm atmosphere due to the faster formation of this radical *via* $H+C_2H_2$ (Figure 10), resulting in a lower concentration ~1 mbar. Photolysis of HCN still yields CN, yet in the $H_2$-dominated atmospheres, reactions to $C_2H_2$ act as the primary production pathway to $HC_3N$ and $C_2H_3CN$, resulting in a narrower production peak near 0.1 μbar (due to the results of $C_2H_2$ shown in 3.2.3).

### 3.2.4 Ethylene, $C_2H_4$

At Titan, $C_2H_4$ is formed from the reaction $CH+CH_4$ and lost to photolysis which yields $C_2H_2$ and either $H_2$ or 2H. The $CH_3$-$CH_4$ exchange described in 3.2.1 encourages the production of CH, thereby increasing the production rate of $C_2H_4$ in the warm $H_2$ atmosphere.

In addition to photolysis, in the $H_2$ atmospheres, $C_2H_4$ is lost to reactions with $H_2$ to form $C_2H_5$, and in the upper atmosphere, the latter reacts with H to form $2CH_3$. In the warm $H_2$ atmosphere, the $CH_3$ may cycle back to methane, photolyze, and further encourage the production reaction $CH+CH_4$. The rates of these reactions are shown in Figure 11.

## 4 GJ 1132b: A warm $H_2$ atmosphere at a close-in orbit around an M-Dwarf

Thus far we have examined, individually, the effect of changing the temperature, host star, semi-major axis, and

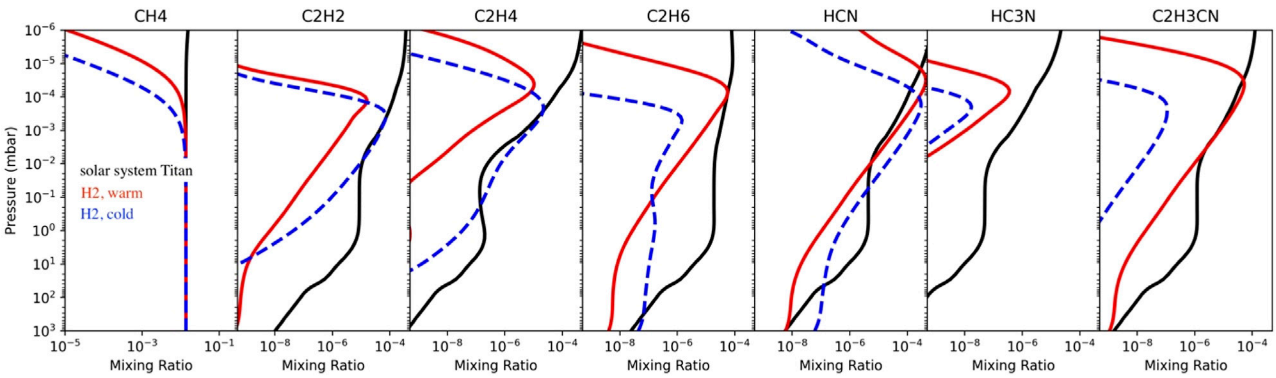


FIGURE 7
Response to temperature and $H_2$ content; all cases are around a Sun-like star at 9.5 AU. Solid black lines: Titan temperature, $N_2$ dominated atmosphere; red lines: warm, $H_2$ dominated atmosphere; blue lines: Titan temperature (cold), $H_2$ dominated atmosphere. From left to right, the panels show $CH_4$, $C_2H_2$, $C_2H_4$, and $C_2H_6$.

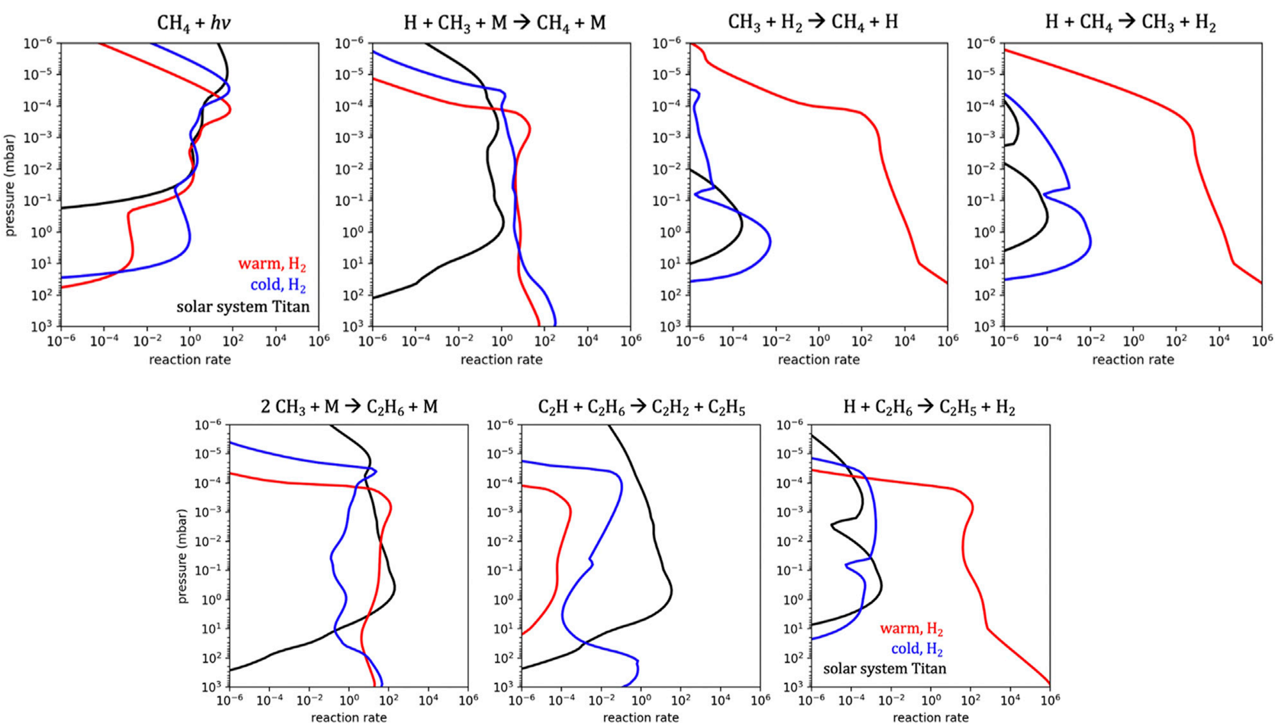


FIGURE 8
Reaction rates ($cm^{-3} \cdot s^{-1}$) of $CH_4$-$CH_3$ recycling and dominant production and destruction reactions for $C_2H_6$. Black lines represent a cold $N_2$ atmosphere (Titan), blue lines represent a cold $H_2$ atmosphere, and red lines represent a warm $H_2$ atmosphere.

stellar type. GJ 1132b is an interesting world with all of these parameters differing from the solar system Titan. Hubble Space Telescope (HST) observations revealed a warm (stratospheric T of 480 K), $H_2$-dominated atmosphere in an otherwise Titan-like atmosphere (90% $H_2$, 8.9% $N_2$, 0.3% HCN, 0.3% $CH_4$, 0.3% CO; Swain et al., 2021), and the world orbits an M-Dwarf at a close-in orbit of 0.01 AU (Bonfils et al., 2018).

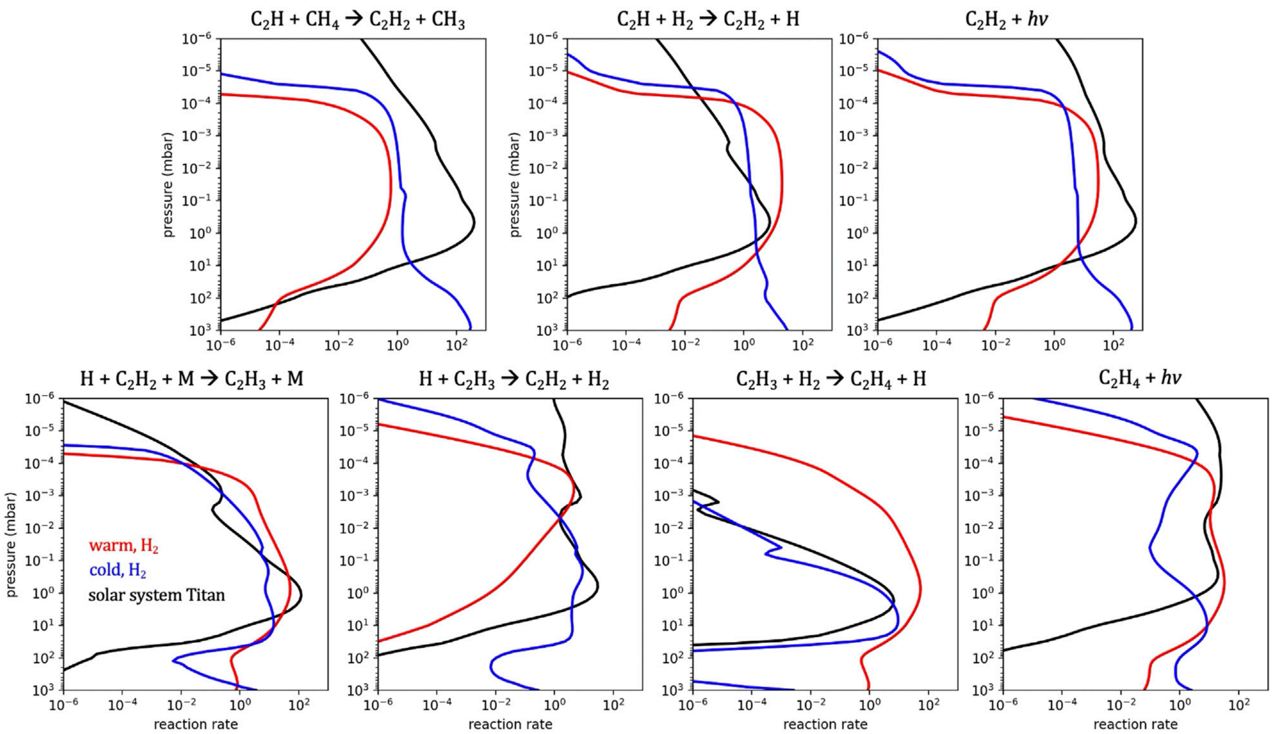


FIGURE 9
Rates ($cm^{-3} \cdot s^{-1}$) of dominant production and loss reactions for $C_2H_2$ in the top panel. Rates of exchange reactions between $C_2H_2$-$C_2H_3$-$C_2H_4$ in the bottom panel. Black lines represent a cold $N_2$ atmosphere (Titan), blue lines represent a cold $H_2$ atmosphere, and red lines represent a warm $H_2$ atmosphere.

Figure 12 shows that the $C_2H_2$ profile peaks just above 0.1 mbar, or near 1,000 km. Above the peak, the rate of formation is limited by the rate of methane photolysis of (due to a low number density). Centered near the peak, the fate $C_2H_2$ is photolysis to $C_2H$, which may cycle back into $C_2H_2$. But, below the peak $C_2H_2$ is lost to reactions with H to yield $C_2H_3$, which may either cycle back to $C_2H_2$ or build larger hydrocarbons. The latter means reactions with H act as a more efficient net loss of $C_2H_2$ than photolysis, hence decreasing the mixing ratio profile of $C_2H_2$ in the regions below.

The $C_2H_4$ profile is comparable to that at Titan as shown in Figure 12. At a close-in orbit around an M-Dwarf, photolysis of methane is efficient and thus synthesis of $C_2H_4$ *via* CH+$CH_4$ is fast. Meanwhile, photolysis of $C_2H_4$ (the main loss) is also efficient. Hence, the production and loss rates have been altered comparably and hence the steady state abundance of $C_2H_4$ is not majorly changed.

We find a depletion in the $C_2H_6$ profile due to the $CH_3$-$H_2$ exchange reactions which efficiently recycle $CH_3$ back to methane before two $CH_3$ molecules may react to form $C_2H_6$. Figure 13 summarizes the new chemical pathways found, starting from Titan (black arrows) and modifying to different host stars, orbital distances, temperatures, and H2:N2 compositions (colored arrows).

# 5 Discussion

## 5.1 Model validation

In this work, we extrapolate the known photochemistry of Titan (e.g., Willacy et al., *accepted*) to putative super-Earth conditions which will become testable in the new JWST era. In order to ensure valid predictions, we validate our model against atmospheric observations of the Titan atmosphere (Figure 14). Our lower boundary conditions of $CH_4$ are based on observations, forcing the lower atmosphere to agree with near-surface observations. The resulting photochemically produced hydrocarbons and N-bearing species roughly agree with the measurements from ALMA and Cassini. Our model overestimates the HCN profile in the lower atmosphere, which we speculate may be related to condensation processes, but the profile roughly matches in the upper atmosphere. Overall, the success of our model reproducing the observations in most regions demonstrates that our predictions of putative super-

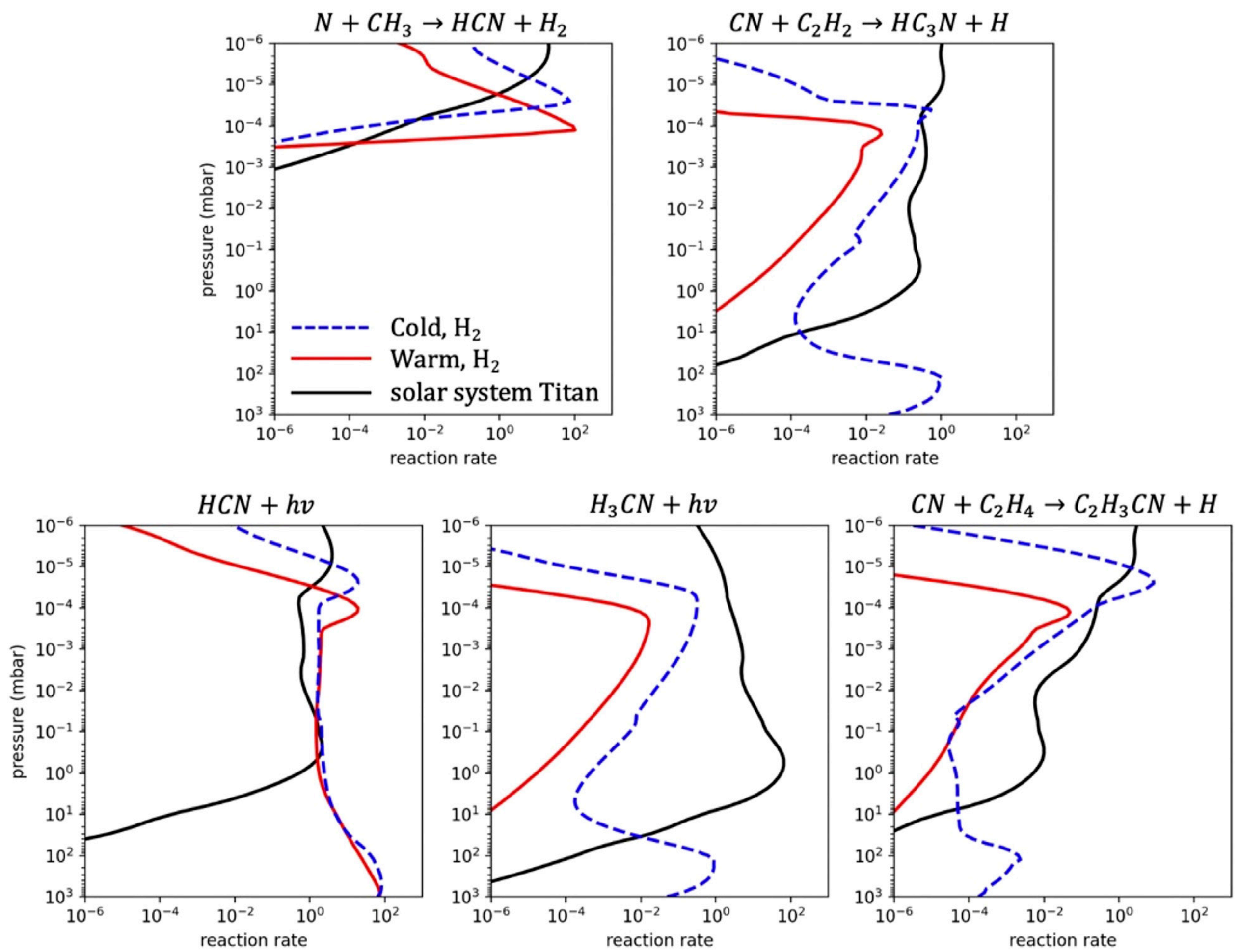


FIGURE 10
Rates ($cm^{-3} \cdot s^{-1}$) of dominant production and loss reactions for -CN species. Black lines represent a cold $N_2$ atmosphere (Titan), blue lines represent a cold $H_2$ atmosphere, and red lines represent a warm $H_2$ atmosphere.

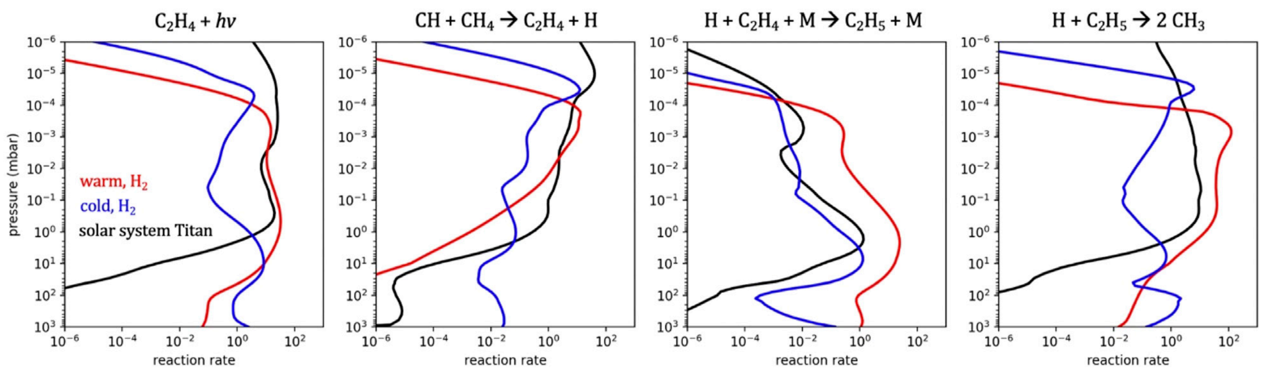


FIGURE 11
Rates ($cm^{-3} \cdot s^{-1}$) of dominant production and loss reactions for $C_2H_4$. Black lines represent a cold $N_2$ atmosphere (Titan), blue lines represent a cold $H_2$ atmosphere, and red lines represent a warm $H_2$ atmosphere.

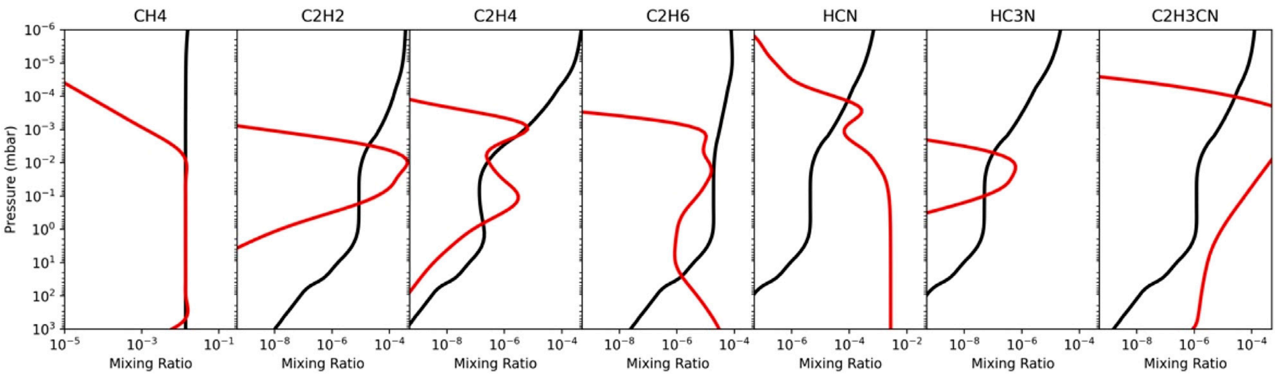


**FIGURE 12**
GJ 1132b (red lines; warm, $H_2$ dominated atmosphere at 0.01 AU away from an M-Dwarf host star) vs. Titan (black lines; cold, $N_2$ dominated atmosphere at 9.55 AU away from the Sun). From left to right, the panels show $C_2H_2$, $C_2H_4$, and $C_2H_6$.

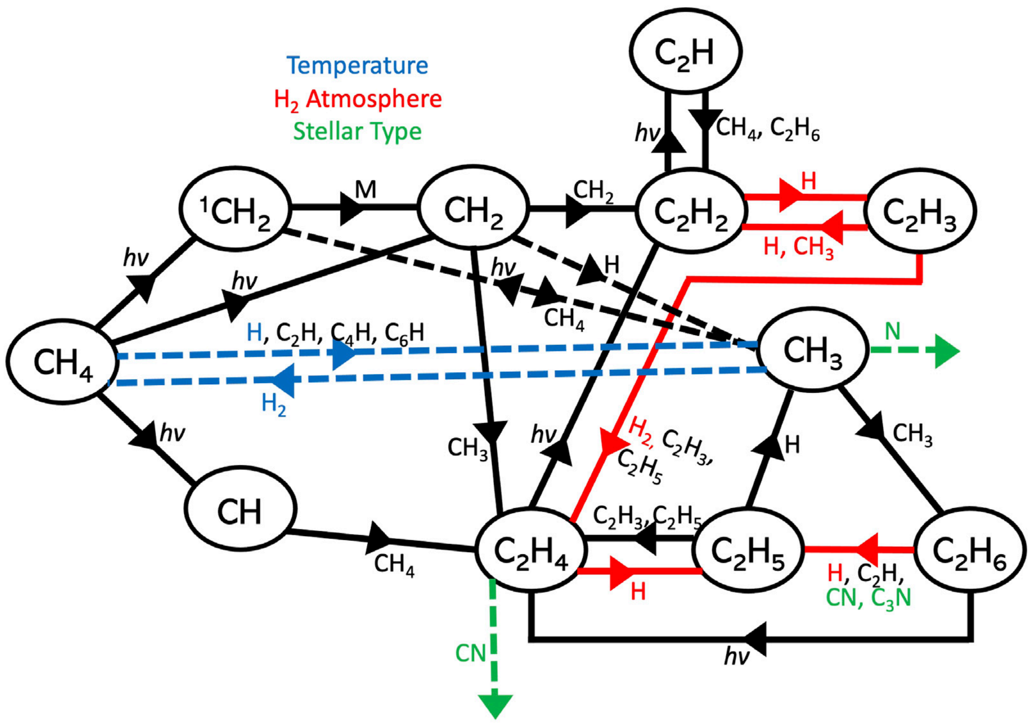


**FIGURE 13**
Diagram of important reactions relevant to hydrocarbon chemistry at Exo-Titans, based off the Titan chemistry presented in Yung et al. (1984). Reactions highlighted in blue show those with a large temperature dependence, thus dominating the chemistry in warmer atmospheres. Reactions highlighted in red show those which become significant in $H_2$-dominant atmospheres. Reactions highlighted in green show those which become significant at worlds around M-Dwarves.

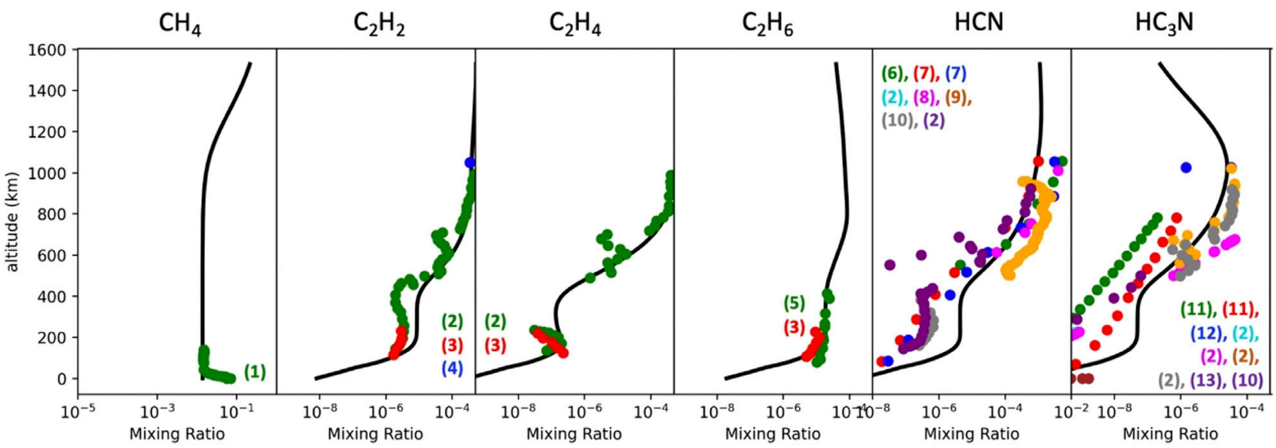


FIGURE 14
Mixing ratio profiles of $CH_4$, $C_2H_2$, $C_2H_4$, $C_2H_6$, HCN, and $HC_3N$ at Titan. Model results are in black and overplotted dots show a comparison to recent observations in the literature: (1) Niemann et al. (2010); (2) Koskinen et al. (2011); (3) Nixon et al. (2013); (4) Magee et al. (2009); (5) Lombardo et al. (2019); (6) Adriani et al. (2011); (7) Kim et al. (2005); (8) Shemansky et al. (2005); (9) Vervack et al. (2004); (10) Vinatier et al. (2010); (11) Cordiner et al. (2014); (12) Cui et al. (2009); (13) Marten et al. (2002)

Earth atmospheres are grounded in a complete photochemical model.

## 5.2 Aerosols

Photochemical hazes are common in reducing atmospheres, as a result of methane and hydrocarbon destruction by solar UV photons and high-energy ions and neutrals, followed by polymerization of the radical species products. Hazes play important roles in radiative transfer, atmospheric dynamics, and atmospheric composition (e.g., Zhang et al., 2017), and they are predicted in atmospheres cooler than ~1000 K (e.g., Gao et al., 2017). Therefore, hazes are common at solar system worlds with reduced atmospheric chemistry, having been revealed at Titan by Voyager (West et al., 1983; West and Smith, 1991) and Cassini (e.g., Tomasko et al., 2008; Lavvas et al., 2009; 2010), Pluto by New Horizons (e.g., Gao et al., 2017; Cheng et al., 2017; Fan et al., 2021), and Triton (e.g., Ohno et al., 2021). Photochemical hazes are also common at exoplanets and influence observables by acting as grey absorbers and muting spectral features (e.g., Adams et al., 2019; Kawashima and Ikoma, 2019; Zahnle et al., 2016; Marley et al., 2013).

Our photochemical models predict notable photochemical production rates of haze material, assuming a soot (hydrocarbon-based) or tholin (N-bearing, hydrocarbon-based) composition. We find rates similar to the production rate at Titan regardless of stellar type or $H_2$ atmospheric content: 2.2e9 molecules $cm^{-2}\cdot s^{-1}$ at Titan; 2.5e9 molecules $cm^{-2}\cdot s^{-1}$ at a 2 AU orbit around an M Dwarf; 1.2e9 molecules $cm^{-2}\cdot s^{-1}$ at a 5.6 AU orbit around a K star; 3.4e9 molecules $cm^{-2}\cdot s^{-1}$ for a warm $H_2$ atmosphere; and 3.4e9 molecules $cm^{-2}\cdot s^{-1}$ for a cool $H_2$ atmosphere. However, the close-in orbits (e.g., GJ 1132b) host large photolysis rates of 8.0e13 molecules $cm^{-2}\cdot s^{-1}$ due to the greater flux of incident photons. The particle sizes are known to scale with production rate (controlled by this preceding photochemistry), which the role of hazes on radiative transfer is dependent on. A larger production rate could lead to more particles available to coagulate, resulting in larger particles. This result may skew observations by muting spectral features, although we note that other parameters may influence the microphysics of particle growth (such as gravity influencing sedimentation, dynamics influencing upward diffusion, and particle fractal dimensions influencing radiative transfer).

## 5.3 Relevance to laboratory measurements

Photochemically derived tholin-like hazes are predicted in the atmosphere of Titan and Titan-like worlds. While haze properties have been derived from atmospheric measurements and compared to numerical models (e.g., Tomasko et al., 2008), the chemical composition of these hazes has not yet been measured at Titan. Laboratory experiments have attempted to constrain the composition by varying parameters including the bulk atmospheric composition, energy sources, trace gases present, temperature (e.g., Khare et al., 1981; Imanaka et al., 2004, 2012; Yoon et al., 2014). Importantly, these works find that tholin-like hazes are meaningful to astrobiology, acting as precursors to amino

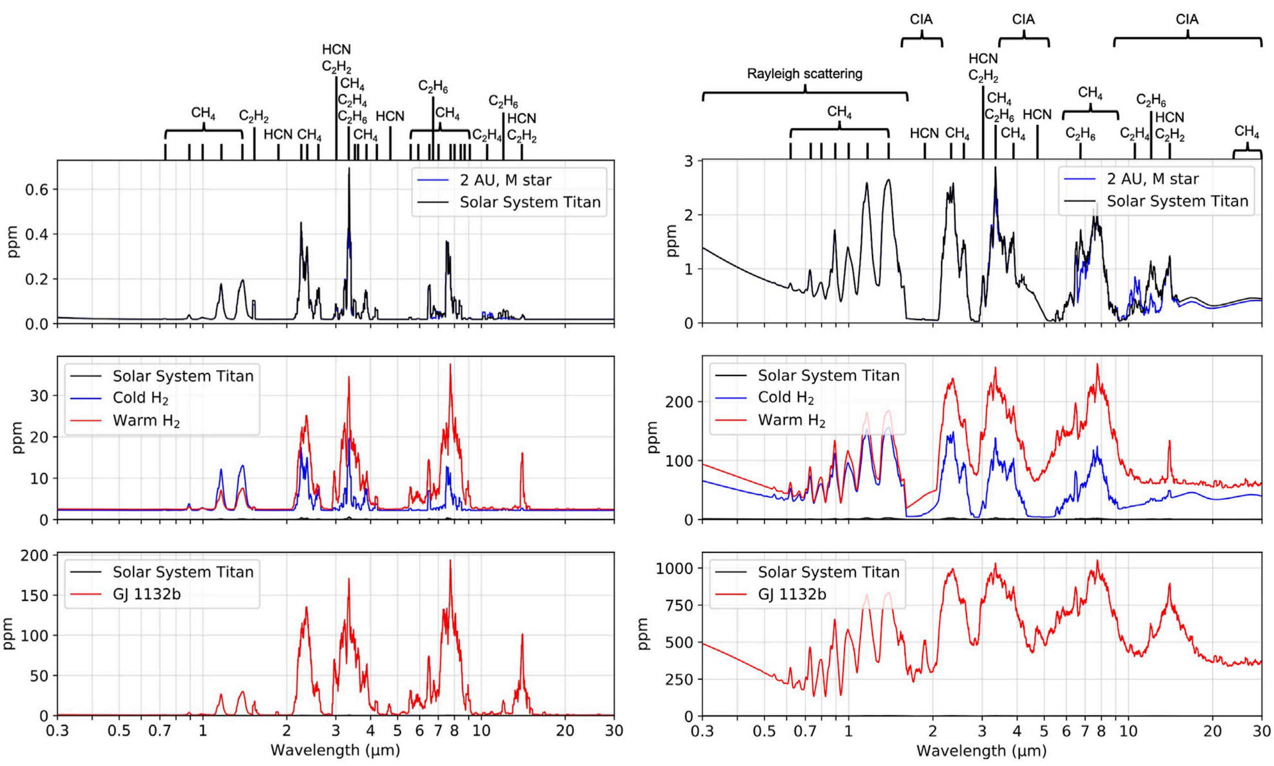


**FIGURE 15**
Computed transmission spectra for the bookend exo-Titan cases presented in this paper (upper) solar system Titan vs. a 2 AU orbit around an M star; (middle) solar system Titan vs. a cold $H_2$-dominated atmosphere (blue) vs. a warm $H_2$ dominated atmosphere (red); (lower) solar system Titan vs. GJ 1132b. Notice the different *y*-axis scales, where the spectral features in the upper panel are well below detection thresholds and spectral features in the middle and the lower panels are much larger and potentially detectable with JWST. The absorption regions of detectable species are labeled above the uppermost panel. CIA, collision-induced absorption.

acids and prebiotic chemistry (e.g., Cable et al., 2012; references therein). For example, after creating tholins in a laboratory environment with a Titan-like background gas composition, hydrolysis was found to yield amino acids including alanine, glutamine, glycine, aspartic acid, and glutamic acid on timescales of a few months (Neish et al., 2010). Similarly, Horst et al. (2012) detected nucleobases and amino acids (including adenine, guanine, uracil, thymine, and cytosine) when exposing a Titan-like laboratory environment to electric discharges. Urea and glycine were also produced in a lab with reducing conditions exposed to electric discharge and plasma impact (Civis et al., 2017). Note that HCN is thought to be an important intermediate which may lead to the formation of nucleobases. Ferus et al. (2017a) find large amounts of HCN and formamide, and the latter is an unstable intermediate likely to decompose to yield HCN (e.g., Ferus et al., 2017b). The results of our work suggest that close-in exo-Titans (such as GJ 1132b) may form Titan-like hazes much quicker than Titan, and the laboratory results discussed suggest this result may imply a greater production of these prebiotic species.

## 5.4 Predicted observability

The new era of JWST begs the question of whether the predicted concentrations and chemistry found in this work are potentially testable. We find that the predicted concentrations at solar system Titan and Titan around an M-Dwarf are both not likely to be detected due to their atmospheres' small scale height. However, the larger scale height of the $H_2$ dominated atmospheres encourage a more feasible detection of the hydrocarbons and nitrile species. GJ 1132b is an especially interesting world: the large scale height, close-in orbit to a relatively smaller star, and greater concentration of HCN makes for potentially more feasible detections. We find that solar system Titan would yield spectral features of order ~1 ppm, while GJ 1132b could yield spectral features of up to >150 ppm in a hazy sky and up to 1,000 ppm in a clear sky.

We present results assuming both a hazy sky and clear sky at all worlds. As discussed in Section 5.2, observations of Titan reveal tholin-like hazes which would mute spectral features, and our photochemical model predicts a haze production rate several orders of magnitude larger at GJ 1132b thereby worsening the outlook for detectability. A flat or sloped spectrum may be capable of muting the large spectral features predicted for GJ 1132b shown in Figure 15. In these results, we do not solve for the haze parameters, but instead assume an optically thick haze layer whose top is located at 10 Pa (motivated by the vertical extent of Titan's hazes; e.g., Rages and Pollack, 1983; West et al., 2018). Exo-Transmit only considers extinction caused by the atmosphere above this pressure level. However, we note that the larger haze production rate at GJ 1132b (see Section 5.2) may influence the haze properties to deviate from those at Titan.

We adapted PandExo, an open source code which determines the noise floor of JWST observations (Batalha et al., 2017), to GJ 1132b, and we find a noise floor of ~400 ppm for NIRCAM's G395H instrument (acknowledging this value varies with wavelength dependences). Comparing to Figure 15 (bottom left panel), we predict the aerosols would mute spectral features below the noise floor for potential detection at GJ 1132b. The molecular features for the species presented in our work would be detectable in a clear sky at GJ 1132b (bottom right panel); however, we find those conditions to be unlikely provided the large haze production rate (see Section 5.2). While JWST detections of these predictions may be challenging, detection of these signals will likely be possible with future instruments dedicated for atmospheric characterization of transiting exoplanets.

## 6 Conclusion

A larger $H_2$ abundance and warmer temperature increases the rate of the back reaction $H_2$+$CH_3$ → $CH_4$+H, and the temperature dependence is so great that $CH_3$ recycles back into $CH_4$ instead of forming $C_2H_6$. A larger $H_2$ abundance and warmer temperature also encourages interesting cycling between $C_2H_2$, $C_2H_3$, and $C_2H_4$ *via* reactions with atomic H. This results in a decreased column abundance of $C_2H_6$ and $C_2H_2$ and relatively larger column abundance of $C_2H_4$ at close-in Exo-Titans with warm, $H_2$-dominant atmospheres than Titan, at a more distant orbit with a cool, $N_2$-dominant atmosphere. Meanwhile, close-in orbits around stars with greater shortwave photon emission result in faster $N_2$ photolysis and a greater availability of HCN, $HC_3N$, and $C_2H_3CN$. We find these abundances may be detectable at close-in, $H_2$ dominated atmospheres (e.g., GJ 1132b) should these worlds have clear skies, but we caution the reader of large haze production rates which may mute these spectral features.

## Data availability statement

The original contributions presented in the study are included in the article/supplementary material, further inquiries can be directed to the corresponding author.

## Author contributions

DA and YL developed the research concept and contributed to drafting and editing the manuscript. DA performed the model simulations.

## Funding

DA was supported by NASA's FINESST program under Proposal Number 80NSSC19K1548. YL was supported in party by funding from NASA's Astrobiology Institute's proposal "Habitability of Hydrocarbon Worlds: Titan and Beyond" (PI: R.M. Lopes of JPL).

## Acknowledgments

We thank Karen Willacy, Mark Swain, and Randy Gladstone for providing helpful discussions which greatly helped this work.

## Conflict of interest

The authors declare that the research was conducted in the absence of any commercial or financial relationships that could be construed as a potential conflict of interest.

## Publisher's note



## References

Adams, D., Gao, P., de Pater, I., and Morley, C. (2019). Aggregate hazes in exoplanet atmospheres. *Astrophys. J.* 874, 1. doi:10.3847/1538-4357/ab074c

Adriani, A., Dinelli, B., Lopez-Puertas, M., Garcia-Comas, M., Moriconi, M., D'Aversa, E., et al. (2011). Distribution of HCN in Titan's upper atmosphere from Cassini/VIMS observations at 3μm. *Icarus* 214 (2), 584–595. doi:10.1016/j.icarus.2011.04.016

Batalha, N., Mandell, A., Pontoppidan, K., Stevenson, K., Lewis, N., Kalirai, J., et al. (2017). PandExo: A community tool for transiting exoplanet science with

JWST and HST. *Publ. astronomical Soc. Pac.* 129, 976. doi:10.1088/1538-3873/aa65b0

Bean, J., Raymond, S., and Owen, J. (2020). The nature and origins of sub-neptune size planets. *J. Geophys. Res. Planets* 126, e2020JE006639. doi:10.1029/2020JE006639

Bonfils, X., Almenara, J.-M., Cloutier, R., Wunsche, a., Astudillo-Defru, N., Berta-Thompson, Z., et al. (2018). Radial Velocity follow-up of GJ 1132 with HARPS. A precise mass for planet b and the discovery of a second planet. *Astron. Astrophys.* 618, A142. doi:10.1051/0004-6361/201731884

Cable, M., Horst, S., Hodyss, R., Beauchamp, P., Smith, M., and Willis, P. (2012). Titan tholins: Simulating titan organic chemistry in the cassini-huygens era. *Chem. Rev.* 112 (3), 1882–1909. doi:10.1021/cr200221x

Chachan, Y., and Stevenson, D. (2018). On the role of dissolved gases in the atmosphere retention of low-mass low-density planets. *Astrophys. J.* 854, 21. doi:10.3847/1538-4357/aaa459

Cheng, A. F., Summers, M. E., Gladstone, G. R., Strobel, D. F., Young, L. A., Lavvas, P., et al. (2017). Haze in Pluto's Atmosphere. *Icarus*. 290, 112–133. doi:10.1016/j.icarus.2017.02.024

Civis, S., Knizek, A., Ivanek, O., Kubelik, P., Zukalova, M., Kavan, L., et al. (2017). The origin of methane and biomolecules from a CO2 cycle on terrestrial planets. *Nat. Astron.* 1, 721–726. doi:10.1038/s41550-017-0260-8

Cordiner, M., Nixon, C., Teanby, N., Irwin, P., Serigano, J., Charnley, S., et al. (2014). ALMA measurements of the HNC and HC3N distributions in Titan's atmosphere. *Astrophys. J.* 795 (2), L30. doi:10.1088/2041-8205/795/2/l30

Cui, J., Yelle, R., Vuitton, V., Waite, J., Kasprzak, W., Gell, D., et al. (2009). Analysis of Titan's neutral upper atmosphere from Cassini ion neutral mass spectrometer measurements. *Icarus* 200 (2), 581–615. doi:10.1016/j.icarus.2008.12.005

Eager, J., Reichelt, D., Mayne, N., Hugo, L., Sergeev, D., Ridgway, R., et al. (2020). Implications of different stellar spectra for the climate of tidally locked Earth-like exoplanets. *Astron. Astrophys.* 639. doi:10.1051/0004-6361/202038089

Fan, S., Gao, P., Zhang, X., Adams, D., Kutsop, N., Bierson, C., et al. (2022). A bimodal distribution of haze in Pluto's atmosphere. *Nat. Commun.* 13, 240. doi:10.1038/s41467-021-27811-6

Ferus, M., Kubelik, P., Kniek, A., Pastorek, A., Sutherland, J., and Civis, S. (2017a). High energy radical chemistry formation of HCN-rich atmospheres on early Earth. *Sci. Rep.* 7, 6275. doi:10.1038/s41598-017-06489-1

Ferus, M., Pietrucci, F., Saitta, A. M., Knizek, A., Kubelik, P., Ivanek, O., et al. (2017). Formation of nucleobases in a Miller-Urey reducing atmosphere. *Proc. Natl. Acad. Sci. U. S. A.* 114, 4306–4311. doi:10.1073/pnas.1700010114

France, K., Loyd, R. O. P., Youngblood, A., Brown, A., Schneider, P. C., Hawley, S., et al. (2016). The MUSCLES Treasury Survey I. Motivation and Overview. *Astrophys. J.* 280, 2. doi:10.3847/0004-637X/820/2/89

Freedman, R. S., Lustig-Yaeger, J., Fortney, J., Lupu, R., Marley, M. S., and Lodders, K. (2014). Gaseous mean opacities for giant planet and ultracool dwarf atmospheres over a range of metallicities and temperatures. *Astrophys. J. Suppl. Ser.* 214, 25. doi:10.1088/0067-0049/214/2/25

Freedman, R. S., Marley, M., and Lodders, K. (2008). Line and mean opacities for ultracool dwarfs and extrasolar planets. *Astrophys. J. Suppl. Ser.* 174 (2), 504–513. doi:10.1086/521793

Gao, P., Fan, S., Wong, M., Liang, M.-C., Shia, R.-L., Kammer, J. A., et al. (2017). New Horizons science TeamConstraints on the microphysics of pluto's photochemical haze from new Horizons observations. *Icarus* 267, 116–123. doi:10.1016/j.icarus.2016.09.030

Gladstone, G. R., Hurley, D. M., Retherford, K. D., Feldman, P. D., Pryor, W. R., Chaufray, J.-A., et al. (2010). LRO-LAMP observations of the LCROSS impcat plume. *Sci.* 330, 472–476. doi:10.1126/science.1186474

Horst, S. M., Yelle, R., Buch, A., Carrasco, N., Cernogora, G., Dutuit, O., et al. (2012). formation of amino acids and nucleotide bases in a titan atmosphere simulation experiment. *Astrobiology* 12 (9), 809–817. doi:10.1089/ast.2011.0623

Imanaka, H., Cruikshank, D. P., Khare, B. N., and McCaky, C. P. (2012). Optical constants of Titan tholins at mid-infrared wavelengths (2.5–25μm) and the possible chemical nature of Titan's haze particles. *Icarus* 218 (1), 247–261. doi:10.1016/j.icarus.2011.11.018

Imanaka, H., Khare, B., Elsila, J. E., Bakes, E. L. O., McKay, C. P., Cruikshank, D. P., et al. (2004). Laboratory experiments of titan tholin formed in cold plasma at various pressures: Implications for nitrogen-containing polycyclic aromatic compounds in titan haze. *Icarus* 168 (2), 344–366. doi:10.1016/j.icarus.2003.12.014

Kaspi, Y., and Showman, A. P. (2015). Atmosphere Dynamics of Terrestrial Exoplanets over a wide range of orbital and atmospheric parameters. *Astrophys. J.* 804, 60. doi:10.1088/0004-637X/804/1/60

Kawashima, Y., and Ikoma, M. (2019). Theoretical transmission spectra of exoplanet atmoshperes with hydrocarbon haze: effect of creation, growth, and settling of haze particles. II. Dependence on UV irradiation intensity, metallicity, C/O ratio, eddy diffusion coefficient, and temperature. *Astrophys. J.* 877, 2. doi:10.3847/1538-4357/ab1b1d

Kempton, E. M. R., Lupu, R., Owusu-Asare, A., Slough, P., and Cale, B. (2017). Exo-Transmit: An open-source code for calculating transmission spectra for exoplanet atmospheres of varied composition. *Publ. Astron. Soc. Pac.* 129 (974), 044402. doi:10.1088/1538-3873/aa61ef

Khare, B. N., Sagan, C., Zumberge, J. E., Sklarew, D. S., and Nagy, B. (1981). Organic solids produced by electrical discharge in reducing atmospheres: Tholin molecular analysis. *Icarus* 48 (2), 290–297. doi:10.1016/0019-1035(81)90110-x

Kim, S., Geballe, T., Noll, K., and Courtin, R. (2005). Clouds, haze, and CH4, CH3D, HCN, and C2H2 in the atmosphere of Titan probed via 3 um spectroscopy. *Icarus* 173 (2), 522–532. doi:10.1016/j.icarus.2004.09.006

Kite, E., Fegley, B., Scahefer, L., and Ford, E. (2020). Atmosphere origins for exoplanet sub-neptunes. *Astrophys. J.* 891, 111. doi:10.3847/1538-4357/ab6ffb

Kopparapu, R. K., Ramirez, R., Kasting, J. F., Eymet, V., Robinson, T., Mahadevan, S., et al. (2013). Habitable zones around main-sequence stars: New estimates. *Astrophys. J.* 765, 131. doi:10.1088/0004-637X/765/2/131

Koskinen, T. T., Yelle, R., Snowden, D., Lavvas, P., Sandel, B., Capalbo, F., et al. (2011). The mesosphere and lower thermosphere of Titan revealed by Cassini/UVIS stellar occultations. *Icarus* 216 (2), 507–534. doi:10.1016/j.icarus.2011.09.022

Lavvas, P., Yelle, R. V., and Vuitton, V. (2009). The detached haze layer in Titan's mesosphere. *Icarus* 201 (2), 626–633. doi:10.1016/j.icarus.2009.01.004

Lavvas, P., Yelle, R. V., and Griffith, C. A. (2010). Titan's vertical aerosol structure at the Huygens landing site: Constraints on particle size, density, charge, and refractive index. *Icarus* 210 (2), 832–842. doi:10.1016/j.icarus.2010.07.025

Libby-Roberts, J. E., Berta-Thompson, Z. K., Diamond-Lowe, H., Gully-Santiago, M. A., Irwin, J. M., Kempton, E. M.-R., et al. (2021), arXiv e-prints, arXiv: 2105.10487. Availablr at: https://arxiv.org/abs/2105.10487

Lombardo, N., Nixon, C., Sylvestre, M., Jennings, D., Teanby, N., Irwin, P., et al. (2019). Ethane in Titan's stratosphere from Cassini CIRS far- and mid- infrared spectra. *Astron. J.* 157 (4), 160. doi:10.3847/1538-3881/ab0e07

Lora, J. M., Kataria, T., and Gao, P. (2018). Atmospheric circulation, chemistry, and infrared spectra of titan-like exoplanets around different stellar types. *Astrophys. J.* 853, 58. doi:10.3847/1538-4357/aaa132

Lorenz, R., and Mitton, J. (2008). *Titan unveiled: Saturn's mysterious moon explored*. Princeton, NJ: Princeton Univ. Press.

Lunine, J. I. (2005). in *Meteorites comets and planets: Treatise on geochemistry*. Editor A. M. Davis (Amsterdam: Elsevier), 623.

Lupu, R. E., Zahnle, K., Marley, M., Schaefer, L., Fegley, B., Morley, C., et al. (2014). The atmospheres of earthlike planets after giant impact events. *Astrophys. J.* 784, 27. doi:10.1088/0004-637X/784/1/27

Magee, B., Waite, J. H., Mandt, K. E., Westlake, J., Bell, J., and Gell, D. A. (2009). INMS-Derived composition of Titan's upper atmosphere: Analysis methods and model comparison. *Planet. Space Sci.* 57 (14-15), 1895–1916. doi:10.1016/j.pss.2009.06.016

Marley, M. S., Ackerman, A. S., Cuzzi, J. N., and Kitzmann, D. (2013). "Clouds and Hazes in Exoplanet Atmospheres," in *Comparative Climatology of Terrestrial Planets, Part III: Clouds and Hazes*. Editors S. J. Mackwell, A. A. Simon-Miller, J. W. Harder, and M. A. Bullock (Tucson: University of Arizona Press), 367–392. doi:10.2458/azu_uapress_9780816530595-ch015

Marten, A., Hidayat, T., Biraud, Y., and Moreno, R. (2002). New millimeter heterodyne observations of titan: Vertical distributions of nitriles HCN, HC3N, CH3CN, and the isotopic ratio 15N/14N in its atmosphere. *Icarus* 158 (2), 532–544. doi:10.1006/icar.2002.6897

Merlis, T., and Schneider, T. (2010). Atmospheric dynamics of earth-like tidally locked aquaplanets. *J. Adv. Model. Earth Syst.* 2, 13. doi:10.3894/JAMES.2010.2.13

Mikal-Evans, T., Crossfield, I. J. M., Benneke, B., Kreidberg, L., Moses, J., Morley, C. V., et al. (2021). Transmission spectroscopy for the warm sub-neptune HD 3167c: Evidence for molecular absorption and a possible high-metallicity atmosphere. *Astron. J.* 161, 18. doi:10.3847/1538-3881/abc874

Morley, C. V., Fortney, J. J., Marley, M. S., Zahlne, K., Line, M., Kempton, E., et al. (2015). Thermal emission and reflected light spectra of super earths with flat transmission spectra. *Astrophys. J.* 815, 110. doi:10.1088/0004-637X/815/2/110

Neish, C., Somogyi, A., and Smith, M. (2010). Titan's primordial soup: Formation of amino acids via low-temperature hydrolysis of tholins. *Astrobiology* 10 (3), 337–347. doi:10.1089/ast.2009.0402

Niemann, H. B., Atreya, S. K., Demick, J. E., Gautier, D., Haberman, J. A., Harpold, D. N., et al. (2010). Composition of Titan's lower atmosphere and simple surface volatiles as measured by the Cassini-Huygens probe gas chromatograph mass spectrometer experiment. *J. Geophys. Res.* 115, E12006. doi:10.1029/2010je003659

Nixon, C., Jennings, D., Bezard, B., Vinatier, S., Teanby, N., Snug, K., et al. (2013). Detection of propene in Titan's stratosphere. *Astrophys. J.* 776, L14. doi:10.1088/2041-8205/776/1/l14

Ohno, K., Zhang, X., Tazaki, R., and Okuzumi, S. (2021). *Haze formation on Triton* 912, 1–37. doi:10.3847/1538-4357/abee82

Rages, K., and Pollack, J. (1983). Vertical distribution of scattering hazes in Titan's upper atmosphere. *Icarus* 55 (1), 50–62. doi:10.1016/0019-1035(83)90049-0

Shemansky, D., Steward, A. I., West, R. A., Esposito, L. W., Hallett, J. T., and Liu, X. (2005). The Cassini UVIS stellar probe of the titan atmosphere. *Science* 308, 978–982. doi:10.1126/science.1111790

Shields, A., Ballard, S., and Johnson, J. A. (2016). The habitability of planets orbiting M-dwarf stars. *Phys. Rep.* 663, 1–38. doi:10.1016/j.physrep.2016.10.003

Shields, A., Meadows, V., Bitz, C., Pierrehumber, R. T., Joshi, M., and Robinson, T. (2013). The effect of host star spectral energy distribution and ice-albedo feedback on the climate of extrasolar planets. *Astrobiology* 13, 715–739. doi:10.1089/ast.2012.0961

Swain, M., Estrela, R., Roudier, G., Sotin, C., Rimmer, P., Valio, A., et al. (2021). Detection of an atmosphere on a rocky exoplanet. *Astron. J.* 161, 213. doi:10.3847/1538-3881/abe879

Tomasko, M. G., Doose, L., Engel, S., Dafoe, L. E., West, R., Lemmon, M., et al. (2008). A model of Titan's aerosols based on measurements made inside the atmosphere. *Planet. Space Sci.* 56 (5), 669–707. doi:10.1016/j.pss.2007.11.019

Vervack, R., Sandel, B., and Strobel, D. (2004). New perspectives on Titan's upper atmosphere from a reanalysis of the Voyager 1 UVS solar occultations. *Icarus* 710 (1), 91–112. doi:10.1016/j.icarus.2004.03.005

Vinatier, S., Bezard, B., Nixon, C., Mamoutkine, A., Carlson, R., Jennings, D., et al. (2010). Analysis of Cassini/CIRS limb spectra of Titan acquired during the nominal mission. I. Hydrocarbons, nitriles and CO2 vertical mixing ratio profiles. *Icarus* 205 (2), 559–570.

West, R. A., Hart, H., Simmons, K. E., Hord, C. W., Esposito, L. W., Lane, A. L., et al. (1983). Voyager 2 photopolarimeter observations of Titan. *J. Geophys. Res.* 88 (A11), 8699–8708. doi:10.1029/JA088iA11p08699

West, R. A., Seignovert, B., Rannou, P., Dumont, P., Turtle, E., Perry, J., et al. (2018). The seasonal cycle of Titan's detached haze. *Nat. Astron.* 2, 495–500. doi:10.1038/s41550-018-0434-z

West, R. A., and Smith, P. H. (1991). Evidence for aggregate particles in the atmospheres of Titan and Jupiter. *Icarus*. 90 (2), 330–333. doi:10.1016/0019-1035(91)90113-8

Willacy, K., Allen, M., and Yung, Y. (2016). A new astrobiological model of the atmosphere of titan. *Astrophys. J.* 829, 79. doi:10.3847/0004-637X/829/2/79

Willacy, K., Chen, S., Adams, D., and Yung, Y. (2022). Vertical distribution of cyclopropenylidene and propadiene in the atmosphere of titan. *Astrophys. J.* 933, 230. doi:10.3847/1538-4357/ac6b9d

Wilson, E. H., and Atreya, S. K. (2004). Current state of modeling the photochemistry of Titan's mutually dependent atmosphere and ionosphere. *J. Geophys. Res.* 109, E06002. doi:10.1029/2003JE002181

Yoon, J., Burrows, J. P., Vountas, M., von Hoyningen-Huene, W., Chang, D. Y., Richter, A., et al. (2014). Changes in atmospheric aerosol loading retrieved from space-based measurements during the past decade. *Atmos. Chem. Phys.* 14 (13), 6881–6902. doi:10.5194/acp-14-6881-2014

Yung, Y., Allen, M., and Pinto, J. (1984). Photochemistry of the atmosphere of Titan – comparison between model and observations. *Astrophys. J. Suppl. Ser.* 55, 465. doi:10.1086/190963

Zahnle, K., Marley, M. S., Morley, C. V., and Moses, J. I. (2016). Photolytic Hazes in the Atmosphere of 51 Eri b. *Astrophys. J.* 824, 2. doi:10.3847/0004-637X/824/2/137

Zhang, X., Strobel, D., and Imanaka, H. (2017). Haze heats Pluto's atmosphere yet explains its cold temperature. *Nature* 551 (7680), 352–355. doi:10.1038/nature24465